

# Synergistic Antitumor Activity from Two-Stage Delivery of Targeted Toxins and Endosome-Disrupting Nanoparticles

Xingfang Su,<sup>†,†</sup> Nicole Yang,<sup>‡</sup> K. Dane Wittrup,<sup>‡,§,||</sup> and Darrell J. Irvine\*,<sup>†,§,||,‡,#</sup>

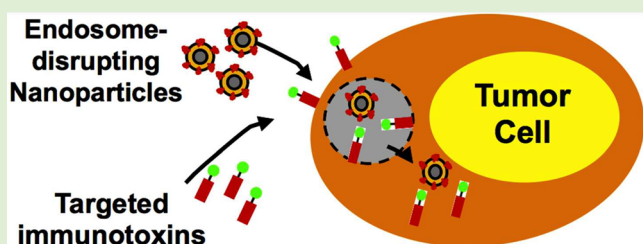
<sup>†</sup>Department of Material Science and Engineering, <sup>‡</sup>Department of Chemical Engineering, <sup>§</sup>Koch Institute for Integrative Cancer Research, and <sup>||</sup>Department of Biological Engineering, Massachusetts Institute of Technology, 77 Massachusetts Avenue, Cambridge, Massachusetts 02139, United States

<sup>‡</sup>Ragon Institute of MGH, MIT, and Harvard, Boston, Massachusetts 02114, United States

<sup>#</sup>Howard Hughes Medical Institute, 4000 Jones Bridge Road, Chevy Chase, Maryland 20815, United States

## Supporting Information

**ABSTRACT:** Plant-derived Type I toxins are candidate anticancer therapeutics requiring cytosolic delivery into tumor cells. We tested a concept for two-stage delivery, whereby tumor cells precoated with an antibody-targeted gelonin toxin were killed by exposure to endosome-disrupting polymer nanoparticles. Co-internalization of particles and tumor cell-bound gelonin led to cytosolic delivery and >50-fold enhancement of toxin efficacy. This approach allows the extreme potency of gelonin to be focused on tumors with significantly reduced potential for off-target toxicity.



## INTRODUCTION

Recent progress in genomics and proteomics has increased our understanding of the molecular basis of many diseases and generated therapeutics based on biomolecules such as peptides, proteins, and nucleic acids that have the potential to fundamentally alter the prognosis of diverse conditions.<sup>1–5</sup> However, compared to conventional small molecule-based drugs that readily diffuse through the cell membrane, such macromolecular drugs often present substantial delivery challenges, stemming from their relative inability to access molecular targets within cells.<sup>6–8</sup> Although cells can internalize polar/high molecular weight molecules via endocytic pathways, this typically results in entrapment within endolysosomal compartments, which leads to fusion with lysosomes and degradation of the endosomal contents without release of significant material to the cytosol. Thus, the endosomal/lysosomal membrane is a barrier to entry into the intracellular space that must be overcome for therapeutics whose function is contingent upon interaction with the cytosolic cellular machinery.

A prominent example of macromolecular drugs requiring cytosolic access for activity are bacterial- and plant-derived toxins—enzymes that carry out lethal biochemistry within the cell and exhibit dramatic potency.<sup>9–12</sup> A few molecules of such toxins in the cytosol are sufficient to kill a cell,<sup>5,10,11</sup> and this high lethality has made these molecules candidate anticancer therapeutics. However, by themselves, type I toxins such as gelonin lacking any cell-binding or cytoplasmic delivery domains are limited by their inability to cross the plasma membrane at therapeutically useful levels.<sup>13</sup> To facilitate cellular uptake as well as tumor-specific killing, these toxins have been

widely explored in the form of immunotoxins, where a targeting moiety specific for a cancer cell (derived from antibodies or other cell-binding proteins) is either chemically conjugated or genetically fused to the highly cytotoxic peptide or protein toxin.<sup>14,15</sup> Nonetheless, the efficacy of such constructs is still dependent on the ability of the toxins to reach their cytoplasmic targets, which remains a significant bottleneck.<sup>16,17</sup> This has fueled the need for the development of appropriately designed cytosolic delivery strategies for these agents.

To date, various synthetic vectors have been investigated for facilitating cytosolic delivery of toxin therapeutics.<sup>18,13,16–19</sup> Many chaperone molecules that efficiently aid transport of macromolecules into the cytosol are formulated with drug cargos by physical complexation or chemical conjugation of the chaperone and drug. In the case of gelonin, a variety of cytosolic delivery strategies have been tested including conjugation to folate, antibodies, peptides, proteins, or polymers, as well as entrapment in liposomes or polymers designed to deliver the toxin to the cytosol of cancer cells.<sup>1–3,6,8,17,20–31</sup> However, the versatility of these existing systems is limited in that the conjugation of the toxin to its chaperone is usually necessary for efficient transduction into cells,<sup>17,24,26,30</sup> the potency of the toxin molecule can be affected by the conjugation, and subsequent release from the chaperone may be required for the toxin to exert its effect.<sup>26,32</sup> One strategy to overcome some of these issues is to conjugate toxins to a polymeric backbone carrier via bonds that are selectively

**Received:** December 25, 2012

**Revised:** February 27, 2013

**Published:** February 27, 2013



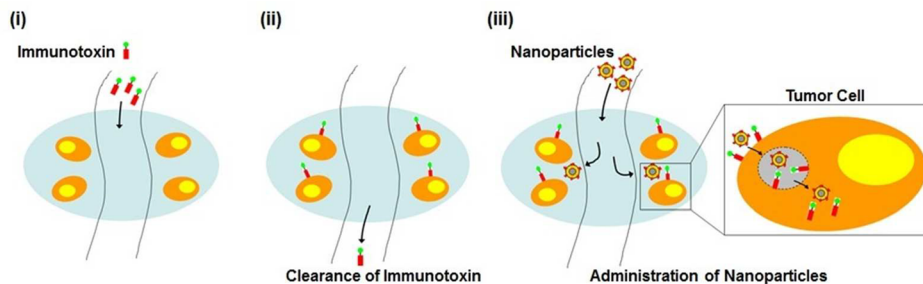


**Figure 1.** Schematic of temporally staggered, staged delivery of a tumor-targeted toxin and a cytosolic delivery chaperone.

cleaved in endolysosomal compartments, so that the immunotoxin drug is released on reaching the target cell.<sup>33</sup> However, a major challenge of all of these toxin conjugate systems remains off-target toxicity, since even low levels of off-target uptake of toxin together with its cytosolic delivery agent lead to cell death and healthy tissue damage.

Underlying each of these approaches is the assumption that successful therapeutic action requires physical association of the toxin and cytosolic entry agent. Here we explore an alternative strategy for temporally staggered, staged delivery of a tumor-targeted toxin and a cytosolic delivery chaperone, which we hypothesize has the potential to achieve effective toxin delivery at a target tumor site while greatly lowering off-target toxicity to nontumor tissue. The proposed two-step approach is outlined in Figure 1: In the first stage, a tumor-targeted (but noncell-permeable) toxin is administered at low doses and allowed time to accumulate on target cells. Antibody-targeted therapeutics are known to provide imperfect tumor targeting, and show uptake in liver and spleen via Fc-mediated binding to phagocytes.<sup>34</sup> However, off-target nonspecific cytoplasmic uptake of the toxin at this stage is minimized by the lack of cytosolic translocation for the targeted toxin on its own. Once the targeted compound has bound to tumor cells but cleared from the systemic circulation and nontarget sites, a chaperoning agent (here, an endosome-disrupting nanoparticle (NP)) is administered as the second stage. Uptake of NPs by toxin-coated tumor cells leads to coendocytic uptake of particles with cell-bound toxin; the particles trigger endosome disruption and release of the toxin for tumor cell killing. Off-target uptake of NPs in the second stage (e.g., in reticuloendothelial system (RES) organs) does not lead to toxicity if the toxin has already been cleared from the extracellular space in these organs. This approach is inspired by pretargeted radioimmunotherapy (PTRIT), where delivery of highly toxic small-molecule radionuclides to tumors is facilitated by administration of a tumor-targeting agent (a bispecific tumor binding/radionuclide-binding antibody) in a first step, followed in a second stage by infusion of a rapidly disseminating small-molecule radionuclide. PTRIT allows the relatively slow tumor uptake/targeting kinetics of the capture bispecific antibody to be temporally separated from the rapid penetration of small-molecule radionuclides throughout the body. Here, instead of temporally staging a capture agent and toxin, we stage delivery of a toxin and a required toxin-activating agent.

We report here in vitro analysis of this concept using soluble or tumor-targeted toxins combined with biodegradable endosome-disrupting nanoparticles as a chaperone agent. For the chaperone particles, we employed pH-responsive lipid-enveloped poly( $\beta$ -amino ester) (PBAE) nanoparticles we recently described that swell in response to acidic pH. These

NPs disrupt endolysosomes and were previously shown to deliver functional mRNA into dendritic cells *in vitro* and *in vivo*.<sup>35</sup> We hypothesized that they would be particularly interesting to test as chaperone agents for delivery of toxins to tumor cells, since recent studies suggest that the elevated metabolic activity of cancer cells makes them dependent on highly active endosome pathways via a process known as autophagy.<sup>36–38</sup> This finding has led to the suggestion that pharmacologic disruption of endosomes/lysosomes may be a useful cytotoxic strategy selective for tumors.<sup>39,40</sup> To this end, we examined in detail the efficiency and limitations of cytosolic drug delivery when a macromolecular cargo of interest (e.g., toxin) is not explicitly bound to the endosome-disrupting agent (the NPs). We found that drug macromolecules in solution (but not bound to the target cell) can be coendocytosed when present in medium together with endosome-disrupting particles, but this process is surprisingly only efficient for cargos of relatively low hydrodynamic radius (<approximately 2–3 nm). In contrast, binding of a (toxin) cargo to the surface of the target cell facilitates efficient coendocytosis with endosome-rupturing NPs added in a second step. NP-mediated delivery of cell-bound toxin into the cytosol enhanced the potency of the type I plant toxin gelonin by more than 50-fold. Altogether, our data suggests that staged delivery of tumor-targeted therapeutics may provide an effective strategy to enhance the potency of toxin therapeutics while improving their safety profile.

## EXPERIMENTAL SECTION

**Materials.** The PBAE poly-1 with a number average molecular weight of ~10 kDa was synthesized as previously reported.<sup>41</sup> The lipids 1,2-dioleoyl-*sn*-glycero-3-phosphocholine (DOPC), 1,2-dioleoyl-3-trimethylammonium-propane (chloride salt) (DOTAP), 1,2-distearoyl-*sn*-glycero-3-phosphoethanolamine-*N*-(methoxy-(poly ethylene glycol)-2000] (ammonium salt) (DSPE-PEG), and 1,2-dioleoyl-*sn*-glycero-3-phosphoethanolamine-*N*-(lissamine rhodamine B sulfonyl) (ammonium salt) (DOPE-rhodamine) were purchased from Avanti Polar Lipids (Alabaster, AL). Calcein was purchased from Sigma Chemical Co. (St. Louis, MO). Fluorescent dextrans (tetramethylrhodamine-labeled 3, 10, 40, or 70 KDa anionic or neutral), unlabeled Phalloidin, and Phalloidin Alexa 488 conjugate were purchased from Invitrogen (Eugene, OR). WST-1 reagent was purchased from Roche Applied Science (Indianapolis, IN). All materials were used as received unless otherwise noted.

**Synthesis and Characterization of Lipid-Coated PBAE Nanoparticles.** Lipid-coated nanoparticles with a poly-1 core were synthesized via a solvent diffusion/nanoprecipitation strategy as previously reported.<sup>35</sup> Briefly, 40 mg of poly-1 (10 KDa, synthesized as previously reported<sup>41</sup>) and 2 mg of the phospholipids DOPC and DOTAP (Avanti Polar Lipids, Alabaster, AL) in a 3.5:1 molar ratio were codissolved in 4 mL of ethanol and added dropwise to 40 mL of distilled, deionized water, followed by gentle stirring for 5 h to

evaporate ethanol. To enable tracking of the particles by fluorescence microscopy, 1 mol % of DOPE-rhodamine was included with the lipids in some experiments. DSPE-PEG was introduced into the lipid coating via a postinsertion process whereby DSPE-PEG lipid was added at 1 mM to 0.5 mg/mL particles in distilled, deionized water, and the suspension was stirred for 16 h at 25 °C followed by washing. The particles were collected and washed once via centrifugation, resuspended in fresh water, and stored at 4 °C until use.

A fraction of each particle batch was dried in a vacuum oven to determine the particle concentration (mg/mL) by measuring the dry mass. Dynamic light scattering (DLS) and zeta potential measurements were used to determine the particle size and surface charge using a ZetaPALS dynamic light scattering detector (Brookhaven Instruments).

**Synthesis of Targeted Gelonins.** The immunotoxins E4rGel and C7rGel, fusion proteins based on the plant-derived toxin gelonin linked to an engineered fibronectin domain targeting the epidermal growth factor receptor (EGFR) or carcinoembryonic antigen (CEA), respectively, were constructed and produced according to previous literature.<sup>39</sup> Briefly, pMal-c2x expression plasmids containing the genes encoding the recombinant form of the gelonin toxin and an engineered fibronectin fragment (based on the tenth human fibronectin type III domain (Fn3)) binding EGFR or CEA were constructed and expressed in Rosetta-gami (DE3) *B. Escherichia coli* cells. The maltose binding protein (MBP)-immunotoxin fusion proteins were subsequently extracted and purified via amylose affinity chromatography. MBP was removed from the immunotoxins by Factor Xa digestion followed by anion-exchange chromatography.

**Cell Culture.** A20 murine lymphoma, B16F10 murine melanoma, A431 human epidermoid carcinoma, and MC38 murine colon carcinoma cells were cultured and passaged in Dulbecco's modified Eagle medium (DMEM) complete medium (10% fetal bovine serum (FBS), 4 mM L-glutamine, 4500 mg/mL glucose, sodium pyruvate, and penicillin/streptomycin). MC38(CEA) cells were maintained under antibiotic selection pressure from Geneticin (0.5 mg/mL).

**Analysis of Endosomal Disruption and Cytosolic Uptake by Confocal Microscopy.** Tumor cells were plated at  $1.2 \times 10^5$  cells/well in Lab-Tek chambers (Nunc) for 18 h, and then calcein (150 µg/mL, 0.24 mM) was added to the cells with or without 75 µg/mL of lipid-coated PBAE nanoparticles in DMEM complete medium (10% FBS, 4 mM L-glutamine, 4500 mg/mL glucose, sodium pyruvate, and penicillin/streptomycin) for 1 h at 37 °C. After washing with medium to remove extracellular calcein/particles, the cells were imaged live under a confocal microscope (Zeiss LSM 510) at 63×.

To study the effects of molecular weight and charge of cargo molecules on cytosolic uptake by cells, B16F10 cells were incubated with labeled dextran (150 µg/mL) with and without nanoparticle (75 µg/mL) for 1 h at 37 °C before washing to remove excess molecules and particles and imaging under a confocal microscope. To quantitatively compare the levels of uptake, the background-subtracted mean fluorescence from replicate fields of view at identical cell densities for each dextran was computed as a measure of total uptake.

**Analysis of Binding of Cargo to Nanoparticles.** To determine the binding of dextran to nanoparticles, dextran (150 µg/mL) was incubated with particles (75 µg/mL) in DMEM containing 10% FBS for 18 h at 37 °C similar to the conditions used during cell treatment. Following adsorption, particles were washed once before resuspending in a digestion buffer (100 mM sodium acetate, 2% triton X-100) to dissolve the particles and disrupt any lipid–dextran complexes. The amount of dextran bound on the particles was then determined by measuring the fluorescence of the resultant solution.

**Staining of Actin Cytoskeleton by Phalloidin and Cytotoxicity Assay.** B16F10 cells were plated as before, and 18 h later, phalloidin (10–25 µM, 5 mol % alexa 488 conjugated) was added to the cells with or without 75 µg/mL of lipid-coated PBAE nanoparticles in DMEM complete medium (10% FBS, 4 mM L-glutamine, 4500 mg/mL glucose, sodium pyruvate, and penicillin/streptomycin) for 3 h at 37 °C. After washing with medium to remove extracellular phalloidin/particles, the cells were imaged live by confocal microscopy.

To assess cytotoxicity, B16F10 cells were plated at  $6 \times 10^5$  cells/well in 12-well plates 18 h prior to experiments. B16F10 cells were then treated with 0, 4, 10, or 25 µM phalloidin alone or with 50 or 75 µg/mL particles in DMEM complete medium for 24 h. After washing with medium to remove extracellular toxin and particles, the cells were detached with Trypsin/ethylenediaminetetraacetic acid (EDTA) and stained with 4',6-diamidino-2-phenylindole (DAPI). The percentage of live cells was quantified via flow cytometry (BD LSR II) by counting cells that were negative for DAPI.

**Cytotoxicity Assay and Analysis via Combination Index.** For the immunotoxin E4rGel, A431 cells, positive for EGFR, were seeded on 96-well plates at 2500 cells/well. Cells were allowed to adhere overnight, after which fresh growth medium (DMEM supplemented with 10% FBS, 4 mM L-glutamine, 4500 mg/mL glucose and sodium pyruvate) containing varying concentrations of immunotoxin and/or particles was added to triplicate wells. Toxins and/or particles were incubated with the cells for up to 24 h before the treatment-containing medium was removed and replaced with fresh medium. At 72 h, medium was replaced with fresh medium containing the WST-1 reagent according to manufacturer's recommendation. The assay was allowed to develop for 1–3 h under normal culture conditions, after which plates were measured for absorbance at 450 nm. Untreated cells and cells lysed with a 1% Triton X-100 solution were used as positive and negative controls, respectively. Measurements were compared with the baseline and normalized to control treatments, triplicates were averaged, and standard errors were calculated. Cytotoxicity measurements were conducted at E4rGel concentrations between  $3 \times 10^{-9}$  and  $3 \times 10^{-8}$  M and particle concentrations between 12.5 and 37.5 µg/mL (particle concentration was reduced accordingly due to the lowered cell density when particle treatment was initiated compared to the earlier assay setups with a shorter time period before readout).

For the immunotoxin C7rGel, MC38 cells, positive or negative for CEA expression, were seeded on 96-well plates at 1000 cells/well. Cells were allowed to adhere overnight, after which fresh growth medium (DMEM supplemented with 10% FBS, 4 mM L-glutamine, 4500 mg/mL glucose and sodium pyruvate, 0.5 mg/mL Geneticin for MC38(CEA) only) containing 1nM immunotoxin (toxin concentration was reduced accordingly due to lower IC<sub>50</sub> of C7rGel ~8 nM relative to E4rGel ~30 nM) was added to triplicate wells. Toxins were incubated with the cells for 3 h, following which the toxin-containing media was removed and the cells were washed with fresh medium before adding titrated doses of PBAE NPs (6.25–25 µg/mL, particle concentration was reduced accordingly due to the lower seeding cell density for the faster growing MC38 cells) that were further incubated with cells for 24 h. The resultant metabolic activity was measured at 72 h as before.

To better assess the enhancement in tumor cell killing by codelivering particles as chaperones for soluble toxin, we analyzed the cytotoxicity data via a combination index that has been previously applied for comparing the efficacy associated with combination therapy (in this case, toxin and particle cotreatment) relative to monotherapy (toxin or particle treatment alone).<sup>42</sup> This is computed as follows: we first calculate the observed percentage of viable cells (% viable cells, observed) in each treatment group normalized to untreated control. We then compute the expected percentage of viable cells in combination treatment groups (% viable cells, combination treatment, expected) by multiplying the percentage of viable cells measured in groups given only particles or toxin at the corresponding concentrations:

$$\% \text{ viable cells, combination treatment, expected}$$

$$= \% \text{ viable cells, particles, observed}$$

$$\times \% \text{ viable cells, toxin, observed}$$

The combination index is defined as:

## Combination index

$$= \frac{\% \text{viable cells, combination treatment, expected}}{\% \text{viable cells, combination treatment, observed}}$$

A ratio of greater than 1 indicates a synergistic effect, while a ratio of less than 1 indicates a less than additive effect.

**Statistical Analysis.** One-way ANOVA followed by Bonferroni's Multiple Comparison Test was applied to determine the statistical significance of differences between groups.

## RESULTS AND DISCUSSION

**Synthesis of Lipid-Coated PBAE NPs.** To achieve cytosolic delivery, we utilized a biodegradable pH-responsive core–shell nanoparticle system we recently developed, composed of a hydrolytically degradable PBAE encased within a biocompatible phospholipid shell (Figure 2).<sup>35</sup> The PBAE

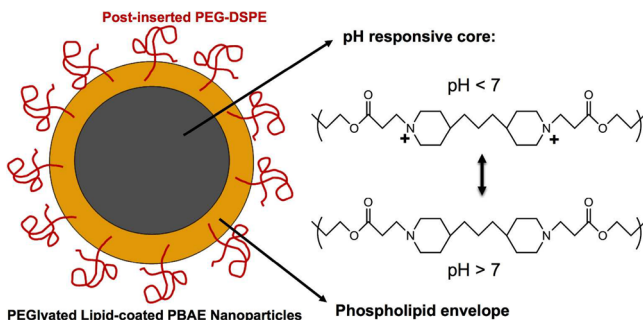


Figure 2. Structure and composition of PEGylated lipid-coated PBAE particles.

core, composed of the PBAE known as poly-1,<sup>41,43</sup> is a weak polyelectrolyte that is water insoluble at elevated pH but ionizes and swells in aqueous solutions below pH ~7 due to the presence of tertiary amine groups in the backbone. This selective ionization/swelling has been exploited to promote cytosolic delivery of drug cargos following uptake by cells,<sup>35,44</sup> which may occur via a “proton sponge effect” and/or dissolution-induced osmotic pressure.<sup>45–47</sup> Here, the core–shell particle structure enables the physical and compositional segregation of particle functions into an endosome-disrupting pH-responsive core and a shell whose composition could be separately tuned to facilitate particle targeting, cell binding, and/or drug binding. The lipid-coated PBAE particles were prepared via a solvent diffusion/nanoprecipitation strategy as previously described.<sup>35</sup> The lipid coating was composed of the phospholipids DOPC and DOTAP in a 3.5:1 molar ratio. To enable tracking of the particles by fluorescence microscopy, 1 mol % of DOPE-rhodamine was included with the lipids in some experiments. DSPE-PEG was introduced into the lipid coating via a postinsertion process, to enhance the colloidal stability of the particles (Figure 2). The resulting particles were  $230 \pm 40$  nm in diameter as determined by dynamic light scattering with a net positive charge as indicated by their zeta potential of  $42 \pm 8$  mV in deionized water.

**Endosomal Disruption and Cytosolic Delivery in Tumor Cells.** In our previous studies with PBAE particles for vaccine delivery, we worked exclusively with dendritic cells, and showed that lipid-enveloped PBAE particles were able to disrupt endosomes and transfect these cells using mRNA while maintaining low toxicity.<sup>35</sup> This result is consistent with several prior studies assessing the viability/metabolic rate of various nontumor cell lines exposed to poly-1 and related PBAE

particles, where low toxicity has made these materials of great interest as gene and drug delivery agents.<sup>48–50</sup> For application in cancer therapy, we first tested whether these particles also mediate endosome disruption in tumor cells. Calcein, a membrane-impermeable fluorophore, was used as a tracer to monitor the stability of endosomes<sup>35,51,52</sup> following particle uptake in two different murine tumor cell lines. A20 lymphoma and B16F10 melanoma cells ( $1.2 \times 10^5$  cells/well) were plated in Lab-Tek chambers for 18 h, and then calcein was added to the cells (150 µg/mL, 0.24 mM) with or without 75 µg/mL of PBAE particles in complete medium (DMEM with 10% FBS) for 1 h at 37 °C. After washing with medium to remove extracellular calcein/particles, the cells were imaged live via confocal microscopy. As shown in Figure 3A, B16F10 cells

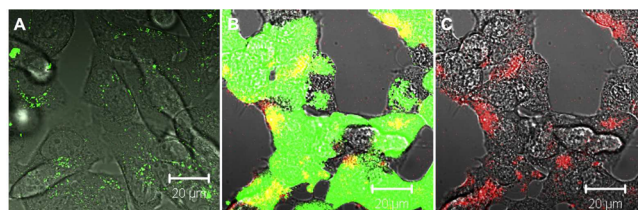
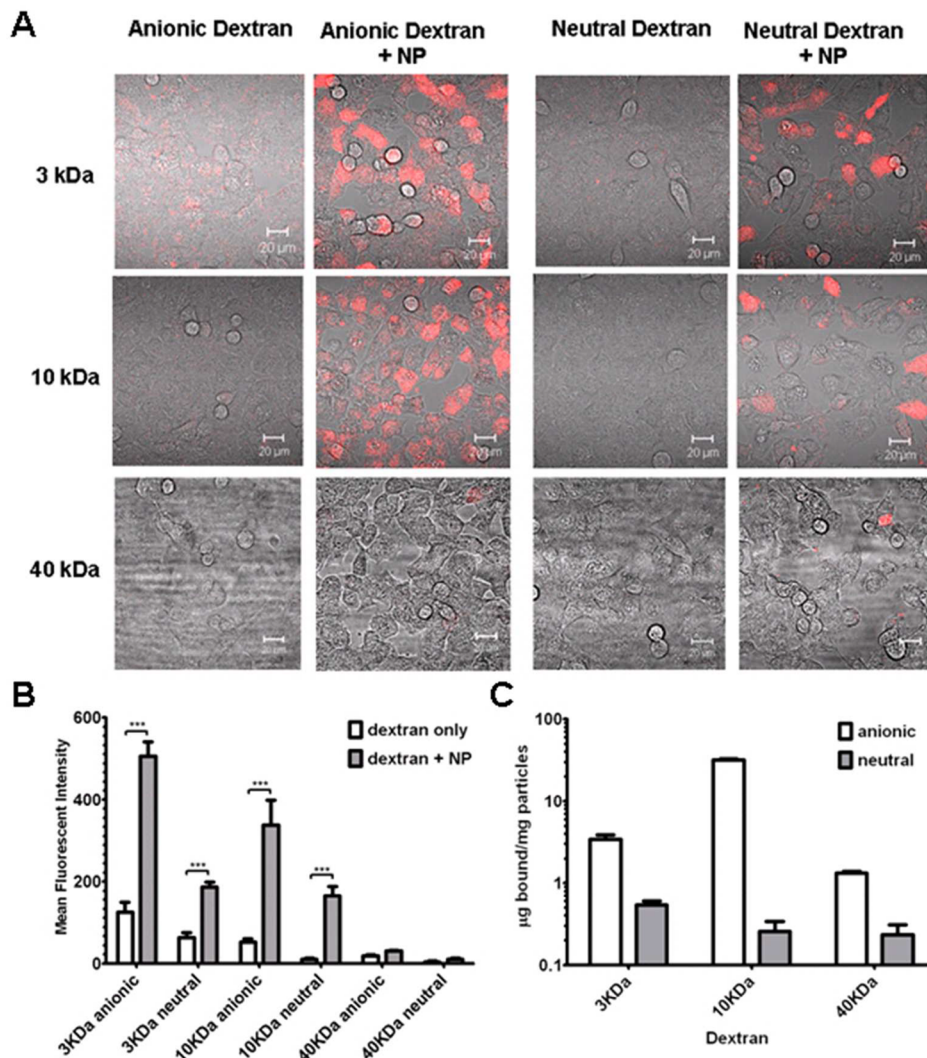


Figure 3. pH-responsive lipid-enveloped PBAE particles disrupt endosomes and deliver coendocytosed calcein into the cytosol and nucleus of tumor cells. B16F10 cells were incubated for 1 h at 37 °C with calcein alone or calcein and rhodamine-labeled lipid-coated PBAE particles, washed to remove unbound particles, then imaged live by confocal microscopy. Representative confocal images of B16F10 melanoma cells incubated with calcein (green) alone (A) or coincubated with calcein and lipid-coated PBAE particles (red, B = brightfield-calcein-particle fluorescence overlay, C = brightfield-particle fluorescence overlay). Scale bars 20 µm.

incubated with calcein alone showed a punctate distribution of fluorescence indicative of endolysosomal compartmentalization of internalized dye. In contrast, cells coincubated with calcein and lipid-enveloped PBAE nanoparticles exhibited calcein fluorescence throughout the cytosol and nucleus, consistent with escape of calcein from intracellular vesicles following cointernalization of extracellular fluid containing both dye and particles (Figure 3B,C). Similar results were observed in A20 lymphoma cells (Figure S1). Previously, we showed that such cytosolic delivery patterns require incubation of PBAE particles and calcein with cells at 37 °C; incubation at 4 °C blocked dye delivery, demonstrating that cytosolic delivery of calcein by these particles is mediated by endosomal uptake followed by endosome disruption and not permeabilization of the plasma membrane.<sup>35</sup> The increase in total internalized calcein fluorescence in cells incubated with particles and calcein versus the dye alone has been observed in multiple systems and is attributable in part to fluorescence quenching as calcein is diluted when the concentrated dye in endosomes is released to the cytosol/nucleus, and also to an increase in the total amount of extracellular fluid internalized by cells during uptake of NPs.<sup>35,53–56</sup> Thus, lipid-enveloped PBAE particles are effectively internalized and disrupt endosomes in tumor cells, similar to our prior findings with immune cells.

**Effect of Molecular Weight and Charge on Cytosolic Delivery of Dextran.** The calcein experiments clearly demonstrate that cells exposed to a membrane-impermeable small molecule compound (calcein molecular weight (MW) 622 Da) and PBAE NPs can efficiently coendocytose the two, leading to release of the small molecule into the cytosol. We



**Figure 4.** Effect of molecular weight and charge of polar cargo macromolecules on cytosolic delivery through coendocytosis with lipid-coated PBAE particles. (A) B16F10 cells were incubated with anionic or neutral fluorescent dextran conjugates (red, 150  $\mu\text{g}/\text{mL}$ ) of various molecular weights, with or without lipid-coated PBAE nanoparticles (unlabeled, 75  $\mu\text{g}/\text{mL}$ ) for 1 h at 37 °C. Cells were washed and imaged live via confocal microscopy. Scale bars 20  $\mu\text{m}$ . (B) Plot of mean fluorescence intensity detected in cells computed from replicate fields of view for each dextran relative to cotreatment with particles (\*\*\*,  $p < 0.0001$ ). (C) Binding of various dextrans to nanoparticles coincubated in DMEM containing 10% serum for 18 h at 37 °C at concentrations identical to the conditions of A and B.

next tested whether polar macromolecular cargos could also be delivered to the cytosol of cells by cotakeup with PBAE NPs from the extracellular environment, and whether the hydrodynamic size of the cargo would influence the result. To probe this, we incubated B16F10 tumor cells for 1 h at 37 °C with fluorescent dextran conjugates (150  $\mu\text{g}/\text{mL}$ ) with molecular weights ranging from 3 KDa to 70 KDa in the absence or presence of particles (75  $\mu\text{g}/\text{mL}$ ), and qualitatively compared the resultant cytosolic uptake by confocal microscopy. The influence of the overall charge of cargo molecules on cytoplasmic uptake was also examined by comparing anionic and neutral dextran conjugates. As shown in Figures 4A,B, dextrans alone were endocytosed at very low levels by B16F10 cells, except for 3 KDa anionic dextran. However, cells coincubated with particles and 3 KDa dextran (both neutral and anionic) displayed enhanced uptake of the polysaccharide in the presence of NPs, coincident with release of the dextran from endosomes, which led to its predominant accumulation in the cytosol. A similar enhancement in polysaccharide uptake

was seen when 10 KDa dextrans were incubated with cells in the presence of PBAE NPs. Neutral 10 KDa dextran released from endosomes by the NPs accumulated in the cytosol similarly to the lower MW polysaccharide, but anionic 10 KDa dextran internalized with NPs remained more punctate in cells, which could reflect binding to the cationic NPs (Figure 4C) or incomplete escape of these charged dextrans from endosomes. (We hypothesize that poly-1 nanoparticles transiently swell in response to endosome acidification, rupture the membrane, and then immediately return to the deswollen state in the neutral pH of the cytosol. In this way, they might remain associated with electrostatically adsorbed dextran during/after endosome disruption.) Notably, at 40 KDa, neither cytosolic delivery nor enhanced uptake of soluble dextran upon particle cotreatment was detected, even with extended overnight incubation. Identical results were observed for a 70 KDa dextran (Figure S2). Although significant binding of dextran to NPs was observed for 10 KDa anionic dextran coincubated with particles in conditions mimicking the cell uptake experiments, relatively

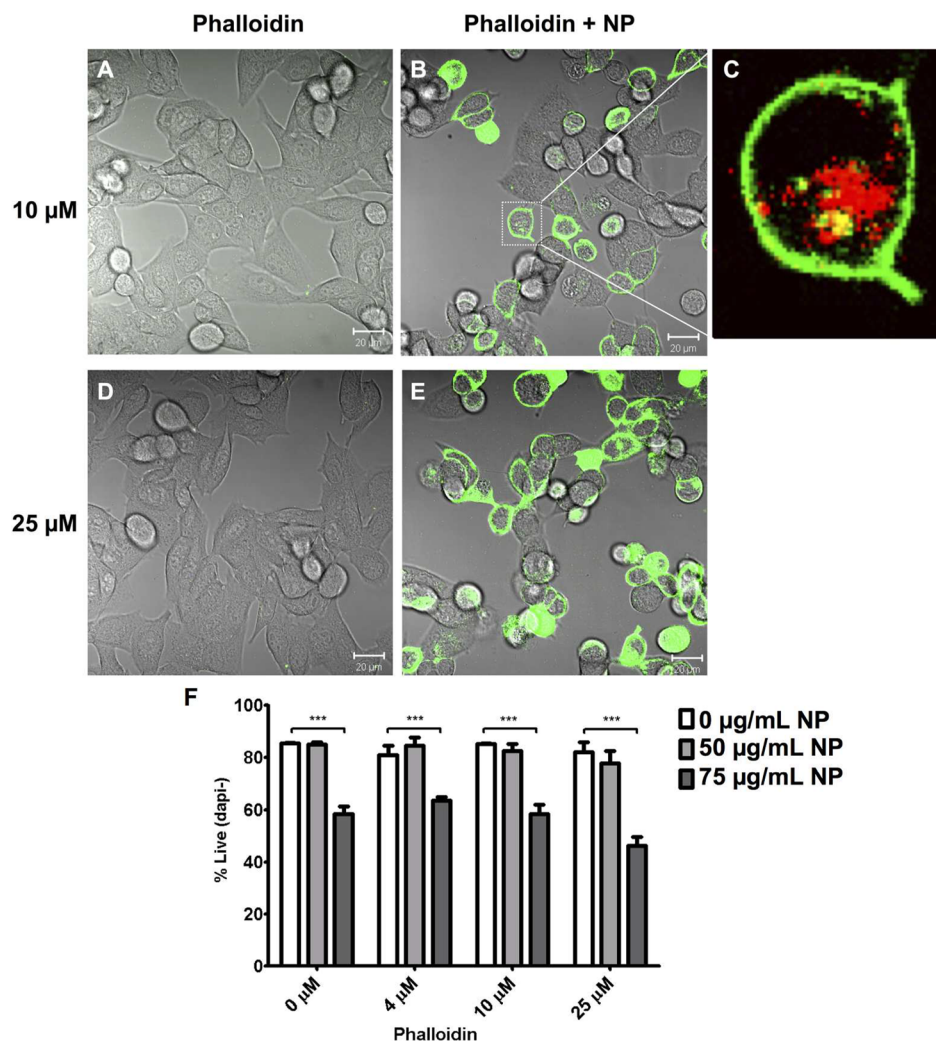


**Figure 5.** Cytosolic delivery of soluble phalloidin by lipid-coated PBAE particles. Confocal images of B16F10 cells incubated with (A) 10  $\mu\text{M}$  or (D) 25  $\mu\text{M}$  phalloidin alone or coincubated with phalloidin and 75  $\mu\text{g}/\text{mL}$  rhodamine-labeled lipid-coated PBAE particles (B–C,E). (A,B,D,E = brightfield-phalloidin fluorescence overlays; C = magnified, phalloidin-particle fluorescence image of boxed cell in B; red, nanoparticles; green, phalloidin-alexa 488 conjugate). (F) Cytotoxicity of B16F10 cells treated with various concentrations of phalloidin alone or combined with 50 or 75  $\mu\text{g}/\text{mL}$  particles for 24 h. (\*\*\*,  $p < 0.0001$ ).

low levels of binding to particles were detected for 3 KDa and 40 KDa anionic dextran (Figure 4C). Furthermore, neutral dextrans of the same molecular weight showed minimal binding to particles but were still effectively chaperoned by particles into cytosol, suggesting that binding to particles is not necessary for the observed particle-mediated cytosolic delivery. On the basis of the hydrodynamic sizes of these polysaccharides, the complete lack of uptake of larger MW dextrans suggests that chaperoning of soluble macromolecular cargos to the cytosol by PBAE NPs will only be efficient for cargos with hydrodynamic radii of approximately 2–3 nm or less. This result is consistent with prior findings of our group and others of particle internalization in cells imaged by transmission electron microscopy, where the cell membrane is observed tightly apposed to the surface of nanoparticles during endocytosis, leaving a gap of only a few nanometers.<sup>52,57,58</sup> As such, we hypothesize that cargos with hydrodynamic diameters exceeding this gap size will be effectively excluded from coendocytic uptake and thereby be poorly chaperoned into cells by PBAE particles.

**Cytosolic Delivery of Phalloidin as a Cytotoxin.** On the basis of the data on dextran/NP coendocytosis, as a first cytotoxic agent for codelivery with NPs, we tested the low molecular weight toxin phalloidin (788 Da), since it is well within the range of molecular sizes where our couptake studies suggested cytosolic delivery should occur. Phalloidin is a cytotoxin isolated from the Death Cap mushroom *Amanita phalloides*; it is a polar, cell-impermeable, cyclic heptapeptide and binds tightly to actin filaments, preventing their depolymerization and thereby poisoning the cell.<sup>59–61</sup> When a sufficient amount of phalloidin is microinjected into the cytoplasm, cell proliferation is inhibited.<sup>62</sup> In a recent study, a pH-responsive cell-penetrating peptide conjugated to phalloidin was shown to facilitate its entry into the cytosol and inhibit the proliferation of cancer cells in a pH-dependent fashion.<sup>63</sup> The actin-binding properties of phalloidin have also made it a common tool for investigating the cytoskeletal organization in cells by labeling phalloidin with fluorescent analogues and using them to visualize actin filaments in microscopy. Incubation of B16F10 cells with Alexafluor-488-(5 mol %) conjugated phalloidin at 10 or 25  $\mu\text{M}$  for 1 h led to negligible uptake of

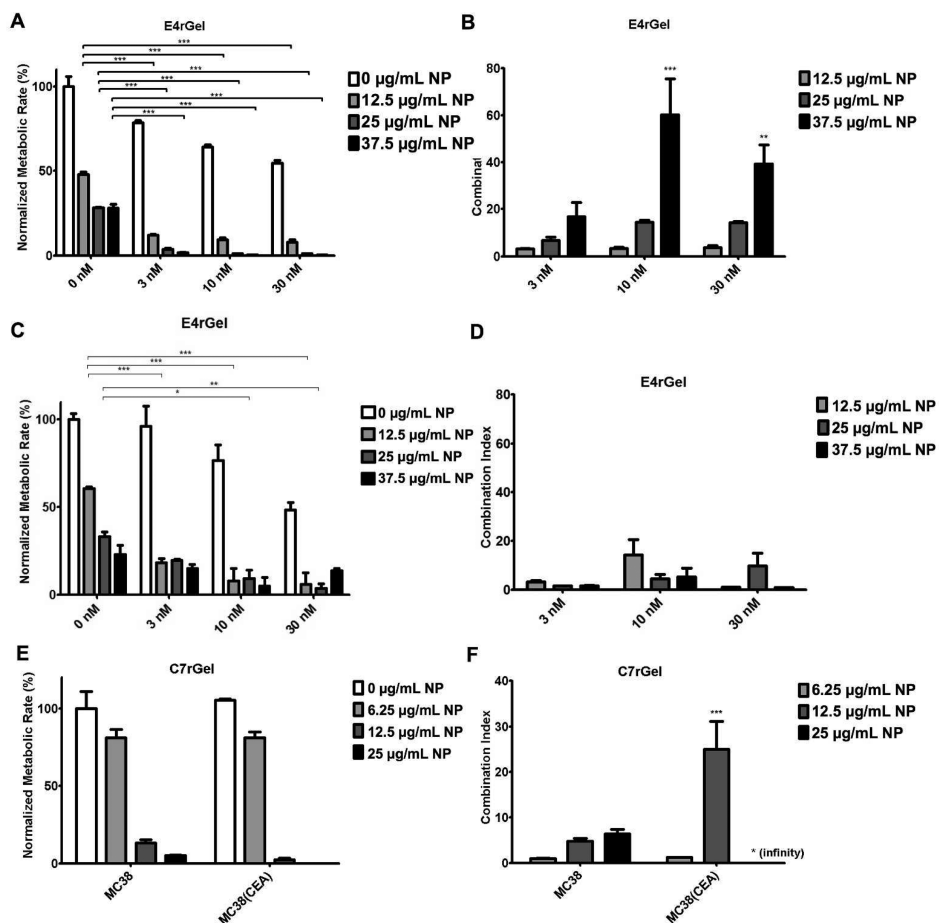


**Figure 6.** Killing of tumor cells by particle-chaperoned immunotoxins. (A–D) Tumor cell lines A431 (EGFR-expressing, A,B) or B16F10 (EGFR-negative, C,D) were incubated with E4rGel immunotoxin and/or lipid-coated PBAE particles at the indicated concentrations for 24 h and then washed into fresh medium. Viability was measured at 72 h via the WST-1 metabolic assay (A,C) and used to compute the combination index where a value  $>1$  indicates synergistic tumor cell killing in the combination treatment (particles + E4rGel) compared to immunotoxin alone (B,D). (E–F) The normalized metabolic rate (E) and combination index (F) for MC38 tumor cells or MC38 cells expressing CEA following incubation with 1 nM of the CEA-targeted C7rGel immunotoxin and lipid-coated PBAE particles at the indicated concentrations. (A: \*\*\*,  $p < 0.0001$ ; B,D: \*\*\*,  $p < 0.0001$ , \*\*,  $p < 0.01$  relative to combination index = 1).

the toxin by the cells (Figure 5A,D). In contrast, coincubation of phalloidin and PBAE NPs led to pronounced toxin uptake. Release of the toxin from endosomes by the NPs led to labeling of the cortical actin cytoskeleton ringing the edge of the membrane in the melanoma cells (Figure 5B,C,E). However, despite clear delivery into the B16 cells, when we measured the cytotoxicity of the NP + phalloidin treatment, no induction of synergistic tumor cell killing was observed (Figure 5F). This may reflect either the modest potency of phalloidin as a cytotoxin and/or resistance of melanoma cells to actin cytoskeletal poisons. However, these data do suggest that low-MW membrane-impermeable therapeutics can be chaperoned into tumor cells efficiently by coadministration with endosome-disrupting nanoparticles, without the requirement for encapsulation or specific binding to the particles to promote uptake. Such a strategy might be particularly useful for local therapy of cancer, where particles and toxin could be coadministered via intratumoral injection.<sup>64–66</sup>

**Synergistic Tumor Cell Killing by Codelivery of Immunotoxins with Nanoparticles.** As phalloidin showed negligible potency in our hands, we looked for a more potent toxin to pair with our endosome-disrupting NPs. In addition, a limitation of mixing nontargeted toxin and free NPs is the

potential for off-target toxicity if particles and toxin were administered systemically and coendocytosed at nontarget tissue sites. Thus, we sought to test a more potent and *targeted* toxin with NPs, to enable the staged delivery concept outlined in Figure 1. To this end, we recently described E4rGel, a 40 kDa (estimated hydrodynamic diameter of ~4–5 nm) immunotoxin comprised of a fusion of gelonin and a fibronectin type III binding domain engineered by directed evolution to exhibit 13 nM affinity for the EGFR.<sup>29</sup> The use of recombinant gelonin in tumor-targeted cytotoxic agents has been studied extensively,<sup>67,68</sup> and EGFR is a well-established cancer-associated antigen commonly used as a target for designed immunotoxins.<sup>9,69</sup> The resultant immunotoxin with engineered fibronectin fragments binding EGFR has an IC<sub>50</sub> of ~30 nM when incubated with EGFR-expressing A431 human epidermoid carcinoma tumor cells for 72 h.<sup>29</sup> This is a significantly lower concentration relative to the μM concentration range reported for phalloidin to achieve antiproliferative effects in tumor cell lines,<sup>63</sup> reflecting the higher potency of targeted gelonin as a cytotoxic agent.

To test whether lipid-enveloped PBAE NPs would amplify the potency of E4rGel, we carried out a cross-titration assay incubating EGFR-expressing A431 tumor cells with the

immunotoxin at a range of concentrations in the presence or absence of titrated doses of PBAE NPs for 24 h, and measured metabolic activity of the tumor cells after 72 h. As shown in Figure 6A, treatment with E4rGel alone at concentrations less than 30 nM resulted in modest levels of cytotoxicity, with cells showing more than 50% of the metabolic rates of untreated controls. This is in agreement with the known inefficiency of endosomal escape, which limits the ability of immunotoxin to reach intracellular targets on its own, as reported previously.<sup>29</sup> Similarly, endosome-disrupting PBAE NPs alone had easily detectable, though modest cytotoxic activity, killing ~75% of the tumor cells following 24 h treatment with 37.5 µg/mL NPs, consistent with the sensitivity of tumor cells to endosome disruption.<sup>39,40</sup> However, the particles combined with immunotoxin were strikingly synergistic: Co-incubation of tumor cells with 3 nM E4rGel and ~40 µg/mL NPs led to essentially complete killing of the tumor cells by 24 h (Figure 6A). To quantify the amplification effect achieved by cotreated cells with the immunotoxin and NPs, we calculated the combination index,<sup>42</sup> a measure of the fold-increase in potency of the combined treatment compared to either treatment alone (see the Experimental section for details of the calculation). As shown in Figure 6B, codelivery of low concentrations of E4rGel and particles resulted in a 60-fold enhancement in potency for 10 nM immunotoxin + ~40 µg/mL NPs following 24 h treatment. By contrast, when we tested E4rGel combined with NPs on control B16F10 tumor cells that lack EGFR expression, we saw similar levels of modest tumor cell killing by the particles alone, but little if any enhancement in NP + toxin treatment groups (Figure 6C,D), suggesting that receptor targeting of the immunotoxin is important for optimal synergistic killing. This extremely high synergy in the combined treatment on EGFR-expressing A431 cells suggests that cytosolic delivery of the targeted toxin is efficient, thereby greatly amplifying the activity of the toxin and providing much greater tumor cell killing than expected from the effect of endosome disruption in the cancer cells alone.

To more cleanly test the importance of targeting toxin to a receptor and to determine whether immunotoxins and NPs could be applied in sequential steps mimicking pretargeted therapy, we next employed another gelonin-based immunotoxin C7rGel, with engineered fibronectin fragments targeting CEA. C7rGel was previously tested on a human fibrosarcoma cell line HT-1080 transfected with a plasmid for CEA expression, demonstrating 10 nM affinity for CEA and an IC<sub>50</sub> of ~8 nM when incubated with CEA-expressing HT-1080 cells for 72 h.<sup>29</sup> C7rGel was used to target the murine colon carcinoma cell line MC38, which was either positive or negative for CEA expression. A staged-delivery approach was adopted for this experiment: antigen-expressing or control MC38 cells were first treated with 1 nM C7rGel for 3 h, following which the toxin-containing media was removed and the cells were washed with fresh medium before adding titrated doses of PBAE NPs that were further incubated with cells for 24 h. Metabolic activity of the treated cells was measured at 72 h and used to compute the combination index as before. As shown in Figure 6C,D, codelivery of C7rGel and particles to antigen-expressing MC38 cells resulted in a 25-fold enhancement in potency relative to particle or immunotoxin monotherapy for 1 nM immunotoxin + 12.5 µg/mL NPs following 24 h treatment, with complete killing of the cells observed for 25 µg/mL NP treatment. Although a modest level of synergy was detected for antigen-negative MC38 cells given the same treatment, the

synergy observed for antigen-expressing cells was more than 5-fold higher for NP concentrations greater than 12.5 µg/mL (note that the combination index is infinity for C7rGel + 25 µg/mL NP due to the complete killing of the tumor cells). Notably, the NP concentrations where synergy is observed here in vitro are well within the range of particle concentrations that are achievable within tumors *in vivo*, given typical treatment doses of 20–30 mg/kg NPs that accumulate in tumors at 5–10% of the injected dose,<sup>70,71</sup> where a rough calculation of treating tumors ~20 mm<sup>2</sup> in diameter gives concentrations of particles in excess of 100 µg/mL in the tumor microenvironment. Together, these data suggest that targeted toxin delivery maximizes the efficacy of subsequent NP treatment under conditions mimicking the staged delivery of tumor therapeutics *in vivo*.

## CONCLUSIONS

In conclusion, we have demonstrated that endosome-disrupting lipid-enveloped PBAE particles are effective as synthetic chaperones to enhance the uptake and cytosolic access of soluble therapeutics, of utility for the delivery of membrane-impermeable toxins for tumor therapy. Simple coadministration of unbound cargo and chaperone allows cointernalization into common endosomes and cytosolic delivery of cargos with hydrodynamic radii ~2–3 nm or smaller, but larger soluble cargos appear to be excluded from endosomes during NP uptake. We further demonstrated the principle of a two-stage delivery of targeted immunotoxins, where targeted toxin is bound to tumor cells in a first stage, followed by addition of NPs that are endocytosed by tumor cells together with cell-bound toxin. Our *in vitro* experiments suggest this approach could achieve highly synergistic enhancement of antitumor activity (more than 50-fold) over that of each component alone. *In vivo*, NPs are well-known to accumulate in tumors via the enhanced permeation and retention effect, and tumor cell uptake can be facilitated by endowing the NPs themselves with tumor-targeting ligands.<sup>72–74</sup> Notably, tumor accumulation of 100–150 nm cationic PBAE nanoparticles encapsulating chemotherapeutics has been previously reported.<sup>75</sup> Because the immunotoxins and NPs have low cytotoxicity alone, off-target uptake of the temporally separated agents in this approach will limit nonspecific toxicity. Such a strategy is of interest for future studies with the targeted gelonin construct. Beyond cancer therapy, the two-stage delivery approach described here may be of broad interest for confining delivery of macromolecular drugs to the cytosol of cells in a defined target tissue.

## ASSOCIATED CONTENT

### Supporting Information

Additional Figures S1 and S2. This information is available free of charge via the Internet at <http://pubs.acs.org/>.

## AUTHOR INFORMATION

### Corresponding Author

\*E-mail: djirvine@mit.edu.

### Present Address

<sup>†</sup>Institute of Materials Research and Engineering, 3 Research Link, Singapore 117602.

### Notes

The authors declare no competing financial interest.

## ACKNOWLEDGMENTS

This work was supported by the Institute for Soldier Nanotechnology (Department of Defense Contract W911NF-07-D-0004). X.S. acknowledges the financial support from the Agency for Science, Technology, and Research, Singapore. D.J.I. is an investigator of the Howard Hughes Medical Institute.

## REFERENCES

- (1) Veenendaal, L. M.; Jin, H. Q.; Ran, S.; Cheung, L.; Navone, N.; Marks, J. W.; Waltenberger, J.; Thorpe, P.; Rosenblum, M. G. *Proc. Natl. Acad. Sci. U.S.A.* **2002**, *99*, 7866–7871.
- (2) Atkinson, S. F.; Bettinger, T.; Seymour, L. W.; Behr, J. P.; Ward, C. M. *J. Biol. Chem.* **2001**, *276*, 27930–27935.
- (3) Cao, Y.; Marks, J. D.; Huang, Q.; Rudnick, S. I.; Xiong, C.; Hittelman, W. N.; Wen, X.; Marks, J. W.; Cheung, L. H.; Boland, K.; Li, C.; Adams, G. P.; Rosenblum, M. G. *Mol. Cancer Ther.* **2012**, *11*, 143–153.
- (4) Leader, B.; Baca, Q. J.; Golan, D. E. *Nat. Rev. Drug Discovery* **2008**, *7*, 21–39.
- (5) Kreitman, R. J.; Pastan, I. *Adv. Drug Delivery Rev.* **1998**, *31*, 53–88.
- (6) Rosenblum, M. G.; Cheung, L. H.; Liu, Y. Y.; Marks, J. W. *Cancer Res.* **2003**, *63*, 3995–4002.
- (7) Li, Z.; Qu, Y.; Li, H.; Yuan, J. *Toxicology* **2007**, *231*, 129–136.
- (8) Lyu, M.-A.; Cao, Y.; Mohamedali, K. A.; Rosenblum, M. G. *Methods Enzymol.* **2012**, *502*, 167–214.
- (9) DiMassimo, A. M.; DiLoreto, M.; Pacilli, A.; Raucci, G.; Dalatri, L.; Mele, A.; Bolognesi, A.; Polito, L.; Stirpe, F.; DeSantis, R. *Br. J. Cancer* **1997**, *75*, 822–828.
- (10) Eiklid, K.; Olsnes, S.; Pihl, A. *Exp. Cell Res.* **1980**, *126*, 321–326.
- (11) Yamaizumi, M.; Mekada, E.; Uchida, T.; Okada, Y. *Cell* **1978**, *15*, 245–250.
- (12) Kuo, C.-L.; Oyler, G.; Shoemaker, C. B. *Toxicon* **2010**, *55*, 619–629.
- (13) Geden, S. E.; Gardner, R. A.; Fabbrini, M. S.; Ohashi, M.; Phanstiel, O. I. V.; Teter, K. *FEBS J.* **2007**, *274*, 4825–4836.
- (14) Pastan, I.; Hassan, R.; FitzGerald, D. J.; Kreitman, R. *J. Nat. Rev. Cancer* **2006**, *6*, 559–565.
- (15) Pastan, I.; Hassan, R.; FitzGerald, D. J.; Kreitman, R. *J. Annu. Rev. Med.* **2007**, *58*, 221–237.
- (16) El-Sayed, M. E. H.; Hoffman, A. S.; Stayton, P. S. *Expert Opin. Biol. Ther.* **2005**, *5*, 23–32.
- (17) Lavignac, N.; Lazenby, M.; Franchini, J.; Ferruti, P.; Duncan, R. *Int. J. Pharm.* **2005**, *300*, 102–112.
- (18) Lai, P.-S.; Pai, C.-L.; Peng, C.-L.; Shieh, M.-J.; Berg, K.; Lou, P.-J. *J. Biomed. Mater. Res., Part A* **2008**, *87A*, 147–155.
- (19) Mastrobattista, E.; Koning, G. A.; van Bloois, L.; Filipe, A. C. S.; Jiskoot, W.; Storm, G. *J. Biol. Chem.* **2002**, *277*, 27135–27143.
- (20) Alam, A.; Bhuri, S. R. K.; Mavila, A. K.; Singh, V. *Mol. Cell. Biochem.* **1992**, *112*, 97–107.
- (21) Better, M. In *Recombinant DNA Biotechnology III: The Integration of Biological and Engineering Sciences*; Asenjo, J. A., Andrews, B. A., Eds.; Annals of the New York Academy of Sciences; New York Academy of Sciences: New York, 1996; Vol. 3, pp 544–554.
- (22) Lambert, J. M.; Senter, P. D.; Yauyoung, A.; Blattler, W. A.; Goldmacher, V. S. *J. Biol. Chem.* **1985**, *260*, 2035–2041.
- (23) McIntosh, D. P.; Heath, T. D. *Biochim. Biophys. Acta* **1982**, *690*, 224–230.
- (24) Patrick, N. G.; Richardson, S. C. W.; Casolaro, M.; Ferruti, P.; Duncan, R. *J. Controlled Release* **2001**, *77*, 225–232.
- (25) Rosenblum, M. G.; Marks, J. W.; Cheung, L. H. *Cancer Chem. Pharm.* **1999**, *44*, 343–348.
- (26) Yuan, X.; Lin, X.; Manorek, G.; Howell, S. B. *BMC Cancer* **2011**, *11*.
- (27) Zhou, H.; Marks, J. W.; Hittelman, W. N.; Yagita, H.; Cheung, L. H.; Rosenblum, M. G.; Winkles, J. A. *Mol. Cancer Ther.* **2011**, *10*, 1276–1288.
- (28) Zhou, X.; Qiu, J.; Wang, Z.; Huang, N.; Li, X.; Li, Q.; Zhang, Y.; Zhao, C.; Luo, C.; Zhang, N.; Teng, X.; Chen, Z.; Liu, X.; Yu, X.; Wu, W.; Wei, Y.-q.; Li, J. *J. Cancer Res. Clin. Oncol.* **2012**, *138*, 1081–1090.
- (29) Pirie, C. M.; Hackel, B. J.; Rosenblum, M. G.; Wittrup, K. D. *J. Biol. Chem.* **2011**, *286*, 4165–4172.
- (30) Lavignac, N.; Lazenby, M.; Foka, P.; Malgesini, B.; Verpilio, I.; Ferruti, P.; Duncan, R. *Macromol. Biosci.* **2004**, *4*, 922–929.
- (31) Provoda, C. J.; Stier, E. M.; Lee, K. D. *J. Biol. Chem.* **2003**, *278*, 35102–35108.
- (32) Arpicco, S.; Dosio, F.; Bolognesi, A.; Lubelli, C.; Brusa, P.; Stella, B.; Ceruti, M.; Cattel, L. *Bioconjugate Chem.* **2002**, *13*, 757–765.
- (33) Zhou, L.; Cheng, R.; Tao, H.; Ma, S.; Guo, W.; Meng, F.; Liu, H.; Liu, Z.; Zhong, Z. *Biomacromolecules* **2011**, *12*, 1460–7.
- (34) Schrama, D.; Reisfeld, R. A.; Becker, J. C. *Nat. Rev. Drug Discovery* **2006**, *5*, 147–59.
- (35) Su, X.; Fricke, J.; Kavanagh, D. G.; Irvine, D. J. *Mol. Pharmaceutics* **2011**, *8*, 774–787.
- (36) Cheong, H.; Lu, C.; Lindsten, T.; Thompson, C. B. *Nat. Biotechnol.* **2012**, *30*, 671–678.
- (37) Lozy, F.; Karantza, V. *Semin. Cell Dev. Biol.* **2012**, *23*, 395–401.
- (38) Maycotte, P.; Thorburn, A. *Cancer Biol. Ther.* **2012**, *11*, 127–137.
- (39) Repnik, U.; Stoka, V.; Turk, V.; Turk, B. *Biochim. Biophys. Acta, Proteins Proteomics* **2012**, *1824*, 22–33.
- (40) Cesen, M. H.; Pegan, K.; Spes, A.; Turk, B. *Exp. Cell Res.* **2012**, *318*, 1245–1251.
- (41) Lynn, D. M.; Langer, R. *J. Am. Chem. Soc.* **2000**, *122*, 10761–10768.
- (42) Dings, R. P. M.; Yokoyama, Y.; Ramakrishnan, S.; Griffioen, A. W.; Mayo, K. H. *Cancer Res.* **2003**, *63*, 382–385.
- (43) Su, X. F.; Kim, B. S.; Kim, S. R.; Hammond, P. T.; Irvine, D. J. *ACS Nano* **2009**, *3*, 3719–3729.
- (44) Lynn, D. M.; Amiji, M. M.; Langer, R. *Angew. Chem., Int. Ed.* **2001**, *40*, 1707–1710.
- (45) Lomas, H.; Massignani, M.; Abdullah, K. A.; Canton, I.; Lo Presti, C.; MacNeil, S.; Du, J. Z.; Blanazs, A.; Madsen, J.; Armes, S. P.; Lewis, A. L.; Battaglia, G. *Faraday Discuss.* **2008**, *139*, 143–159.
- (46) Boussif, O.; Lezoualch, F.; Zanta, M. A.; Mergny, M. D.; Scherman, D.; Demeneix, B.; Behr, J. P. *Proc. Natl. Acad. Sci. U.S.A.* **1995**, *92*, 7297–7301.
- (47) Sonawane, N. D.; Szoka, F. C.; Verkman, A. S. *J. Biol. Chem.* **2003**, *278*, 44826–44831.
- (48) Akinc, A.; Anderson, D. G.; Lynn, D. M.; Langer, R. *Bioconj. Chem.* **2003**, *14*, 979–988.
- (49) Akinc, A.; Lynn, D. M.; Anderson, D. G.; Langer, R. *J. Am. Chem. Soc.* **2003**, *125*, 5316–5323.
- (50) Vandebroucke, R. E.; De Geest, B. G.; Bonne, S.; Vinken, M.; Van Haecke, T.; Heimberg, H.; Wagner, E.; Rogiers, V.; De Smedt, S. C.; Demeester, J.; Sanders, N. N. *J. Gene Med.* **2008**, *10*, 783–94.
- (51) Straubinger, R. M.; Hong, K.; Friend, D. S.; Papahadjopoulos, D. *Cell* **1983**, *32*, 1069–1079.
- (52) Hu, Y.; Litwin, T.; Nagaraja, A. R.; Kwong, B.; Katz, J.; Watson, N.; Irvine, D. J. *Nano Lett.* **2007**, *7*, 3056–3064.
- (53) Dacey, D. M.; Peterson, B. B.; Robinson, F. R.; Gamlin, P. D. *Neuron* **2003**, *37*, 15–27.
- (54) Febvay, S.; Marini, D. M.; Belcher, A. M.; Clapham, D. E. *Nano Lett.* **2010**, *10*, 2211–2219.
- (55) Hamann, S.; Kiilgaard, J. F.; Litman, T.; Alvarez-Leefmans, F. J.; Winther, B. R.; Zeuthen, T. *J. Fluoresc.* **2002**, *12*, 139–145.
- (56) Tenopoulou, M.; Kurz, T.; Doulias, P. T.; Galaris, D.; Brunk, U. T. *Biochem. J.* **2007**, *403*, 261–266.
- (57) Musyanovych, A.; Dausend, J.; Dass, M.; Walther, P.; Mailaender, V.; Landfester, K. *Acta Biomater.* **2011**, *7*, 4160–4168.
- (58) Yue, H.; Wei, W.; Yue, Z.; Lv, P.; Wang, L.; Ma, G.; Su, Z. *Eur. J. Pharm. Sci.* **2010**, *41*, 650–657.
- (59) Delacruz, E. M.; Pollard, T. D. *Biochemistry* **1994**, *33*, 14387–14392.
- (60) Faulstich, H.; Schafer, A. J.; Weckauf, M. *Hoppe-Seylers Z. Physiol. Chem.* **1977**, *358*, 181–184.

- (61) Wieland, T. *Nature* **1977**, *64*, 303–309.
- (62) Wehland, J.; Osborn, M.; Weber, K. *Proc. Natl. Acad. Sci. U.S.A.* **1977**, *74*, 5613–5617.
- (63) An, M.; Wijesinghe, D.; Andreev, O. A.; Reshetnyak, Y. K.; Engelman, D. M. *Proc. Natl. Acad. Sci. U.S.A.* **2010**, *107*, 20246–20250.
- (64) Fisher, B.; Anderson, S. J. *N. Engl. J. Med.* **2007**, *357*, 1051–1051.
- (65) Lo, S. S.; Moffatt-Bruce, S. D.; Dawson, L. A.; Schwarz, R. E.; Teh, B. S.; Mayr, N. A.; Lu, J. J.; Grecula, J. C.; Olencki, T. E.; Timmerman, R. D. *Nat. Rev. Clin. Oncol.* **2011**, *8*, 405–416.
- (66) Morgan, S. C.; Parker, C. C. *Nat. Rev. Clin. Oncol.* **2011**, *8*, 504–506.
- (67) Scott, C. F.; Lambert, J. M.; Goldmacher, V. S.; Blattler, W. A.; Sobel, R.; Schlossman, S. F.; Benacerraf, B. *Int. J. Immunopharmacol.* **1987**, *9*, 211–225.
- (68) Yazdi, P. T.; Murphy, R. M. *Cancer Res.* **1994**, *54*, 6387–6394.
- (69) Beers, R.; Chowdhury, P.; Bigner, D.; Pastan, I. *Clin. Cancer Res.* **2000**, *6*, 2835–2843.
- (70) Jain, R. K.; Stylianopoulos, T. *Nat. Rev. Clin. Oncol.* **2010**, *7*, 653–664.
- (71) Schroeder, A.; Heller, D. A.; Winslow, M. M.; Dahlman, J. E.; Pratt, G. W.; Langer, R.; Jacks, T.; Anderson, D. G. *Nat. Rev. Cancer* **2011**, *12*, 39–50.
- (72) Arias, J. L. *Mini-Rev. Med. Chem.* **2011**, *11*, 1–17.
- (73) Ruoslahti, E.; Bhatia, S. N.; Sailor, M. J. *J. Cell Biol.* **2010**, *188*, 759–768.
- (74) Wang, M.; Thanou, M. *Pharmacol. Res.* **2010**, *62*, 90–99.
- (75) Shenoy, D.; Little, S.; Langer, R.; Amiji, M. *Pharm. Res.* **2005**, *22*, 2107–2114.